Tuning of the FMN binding and oxido-reduction properties by neighboring side chains in *Anabaena* Flavodoxin

Susana Frago[1], Guillermina Goñi[1], Beatriz Herguedas[1], José Ramón Peregrina[1], Ana Serrano[1], Inmaculada Perez-Dorado[2], Rafael Molina[2], Carlos Gómez-Moreno[1], Juan A. Hermoso[2], Marta Martínez-Júlvez[1], Stephen G. Mayhew[3], and Milagros Medina[1]

[1] *Departamento de Bioquímica y Biología Molecular y Celular. Facultad de Ciencias and Institute of Biocomputation and Physics of Complex Systems (BIFI). Universidad de Zaragoza. 50009-Zaragoza. Spain.*

[2] *Grupo de Cristalografía Macromolecular y Biología Estructural. Instituto Química-Física Rocasolano. C.S.I.C. Serrano 119. 28006-Madrid, Spain*

[3] *School of Biomolecular and Biomedical Sciences. UCD Conway Institute, University College Dublin. Belfield. Dublin 4. Ireland.*

Correspondence to: Dr. Milagros Medina. Departamento de Bioquímica y Biología Molecular y Celular. Facultad de Ciencias. Universidad de Zaragoza. 50009-Zaragoza. Spain. Phone: 34976762476 Fax: 34976762123 e-mail: mmedina@unizar.es

Short title: Modulation of FMN properties by the protein environment in flavodoxin

Abbreviations: ox, sq or hq, oxidized, semiquinone or hydroquinone forms of the flavin ring; ET, electron transfer; $E_{ox/sq}$, midpoint reduction potential for the ox/sq couple; $E_{sq/hq}$, midpoint reduction potential for the sq/hq couple; WT, wild-type; P-binding, phosphate-binding; Fld, flavodoxin; ApoFld, apoflavodoxin; Fld_{ox}, Fld in the oxidized state; Fld_{hq}, Fld in the hydroquinone state; Fld_{sq}, Fld in the semiquinone state; K_d, dissociation constant; FNR, ferredoxin-$NADP^+$ reductase; PSI, Photosystem I; ΔG_{ox}, ΔG_{sq}, ΔG_{hq}, free energy of binding for ApoFld:FMN_{ox}, ApoFld:FMN_{sq} and ApoFld:FMN_{hq} complexes.

Summary

Contribution of three regions (phosphate-binding, 50´s and 90´s loops) of *Anabaena* apoflavodoxin to FMN binding and reduction potential was studied. Thr12 and Glu16 did not influence FMN redox properties, but Thr12 played a role in FMN binding. Replacement of Trp57 with Glu, Lys or Arg moderately shifted $E_{ox/sq}$ and $E_{sq/hq}$ and altered the energetic of the FMN redox states binding profile. Our data indicate that the side chain of position 57 does not modulate $E_{ox/sq}$ by aromatic stacking or solvent exclusion, but rather by influencing the relative strength of the H-bond between the N(5) of the flavin and the Asn58-Ile59 bond. A correlation was observed between the isoalloxazine increase in solvent accessibility and less negative $E_{sq/hq}$. Moreover, $E_{sq/hq}$ became less negative as positively charged residues were added near to the isoalloxazine. Ile59 and Ile92 were simultaneously mutated to Ala or Glu. These mutations impaired FMN binding, while shifting $E_{sq/hq}$ to less negative values and $E_{ox/sq}$ to more negative. These effects are discussed on the bases of the X-ray structures of some of the Fld mutants, suggesting that in *Anabaena* Fld the structural control of both electron transfer steps is much more subtle than in other Flds.

Key words: Flavodoxin, FMN reduction potential, FMN binding, X-ray structures

Introduction

Flavodoxins (Flds) are small α/β flavoproteins involved in numerous electron transfer (ET) reactions in prokaryotic organisms and certain algae [1, 2]. Non-covalently bound FMN confers Fld with its ability to act as a low potential electron carrier. Complex formation causes $E_{ox/sq}$ and $E_{sq/hq}$ of FMN to be inverted and to become well-separated [3, 4].

Three main regions of apoflavodoxin (ApoFld) are involved in FMN binding: the phosphate-binding (P-binding) loop, the 50´s loop and the 90´s loop [5, 6]. Although the phosphate group of FMN is charged, electrostatic interactions do not seem to play a major role, and instead the P-binding loop contributes to stabilize phosphate through H-bonds provided by side chains of several Thr (or Ser) and main chain NH groups of the consensus sequence T/S-X-T/S-G-X-T/S-X (10-T-Q-T-G-K-T-E-16 in *Anabaena* Fld) [5-8]. Residues in the 50´s and 90´s loops make close contacts with the isoalloxazine ring and modulate its reduction properties [9-15]. Despite the high sequence similarity between Flds, the structure around the flavin and the specific interactions of the flavin with the ApoFld vary in these loops, tuning different reduction potentials. In most Flds the 90´s loop provides a Tyr stacked against the *si*/outer face of FMN (Tyr94 in *Anabaena*). The residue from the 50's loop that stacks at the *re*/inner face is commonly a Trp, as in *Anabaena* (Trp57) [7, 16-20], but non-aromatic residues have also been found; Leu in *Azotobacter vinelandii* [21] and *Klebsiella pneumoniae* Flds [22], Met in *Clostridium beijerinckii* Fld [3], His in Fld MioC from *E. coli* [23] and Ala in *Helicobacter pylori* Fld [20]. Other side chains at the 50´s loop have also been suggested to play a role in $E_{ox/sq}$ modulation [24]. While the H-bond network observed in *Anabaena* Fld is essentially conserved in Fld structures from different species [25], the 56-60 segment varies considerably [3, 19, 26]. When Flds from *C. beijerinckii* and

Desulfovibrio vulgaris are reduced to the sq, a rearrangement of the 58-59 peptide bond occurs (*Anabaena* numbering), allowing a main chain carbonyl O (contributed by a Gly) to flip from an "O-down" conformation to an "O-up" conformation. In this "O-up" conformation, formation of a H-bond between this main chain carbonyl O and the N(5)H from the neutral sq occurs [27, 28]. In *Anacystis nidulans* Fld (high sequence and structure conservation with *Anabaena* Fld and position 58 is also contributed by an Asn) this flip involves the breaking of a weak H-bond present in the ox state between the FMN N(5) and the NH group of Val59, in favor of the stronger H-bond between the carbonyl group of Asn58 ("O-up" conformation) and FMN N(5)H in the sq state. In *Anabaena* Fld, the NH group of Ile59 is 3.7 Å from N(5) but the orientation presents a favorable geometry that suggests such an H-bond also stabilizes *Anabaena* Fld_{ox} [7]. This loop geometry and N(5) interaction appears common to long-chain Flds from *A. nidulans, E. coli* and *Anabaena*, but has not been found in the long-chain Fld from *Azotobacter vinelandii*, nor in the short-chain Flds from *D. vulgaris* and *C. beijerinckii* [21]. The fact that the sq states of *A. nidulans* and *Anabaena* Flds are less stable than those of Flds from other species has been correlated to the weaker H-bond that is formed between the N(5)H of the flavin and the backbone CO of Asn compared to the bond formed with the smaller Gly and to the presence in the oxidized state of the N(5)-HN59 H-bond that is absent in other Flds [3, 26]. Such backbone rearrangements appear to provide a versatile device for modulating the reduction potential, and a similar role for the Asn58-Ile59 peptide to that found in *A. nidulans* Fld can be predicted in *Anabaena* Fld [24].

Mutational and structural studies can be used to investigate the contributions of an amino acid side chain to modulate the reduction potentials and the binding affinities of the different redox states of FMN. Replacement of Asn58 by Lys in *Anabaena* Fld

decreased the $E_{ox/sq}$ value, effect related to an increase in the conformational energy of the peptide Asn58-Ile59 in the sq state [24]. Ile59 and Ile92 are the only two hydrophobic residues exposed to solvent and situated in the isoalloxazine ring environment where interaction of Fld with its ET partners is expected. Single mutational studies at these positions in *Anabaena* Fld indicated that the nature of these side chains tunes $E_{ox/sq}$ and that these residues appear to play a role in complex formation and ET between photosystem I (PSI) and Fld [29]. The role of *Anabaena* Fld Trp57 in FMN binding and reduction potential tuning has also been analyzed by replacing it with non-charged residues, concluding that it plays a role in FMN binding rather than in redox properties modulation, and that it is involved in setting an appropriate environment to modulate *in vivo* ET from PSI to FNR [9, 30].

In the present manuscript we examine the effect on FMN binding and reduction potentials when residues in the FMN binding site that are thought to be involved in the interaction of Fld with other proteins are modified [30-32]. The highly conserved Thr12 (occurring only as Thr or Ser) and Glu16 (usually Glu or Arg) at the terminal end of the P-binding loop have been mutated to lysine. The effect of introducing charged side chains close to the isoalloxazine moiety of FMN has also been tested by replacing Trp57 with Glu, Lys and Arg. Finally, Ile59 and Ile92 have been simultaneously substituted by Ala and Glu, to investigate the effect of replacing the only surface hydrophobic residues close to the FMN. The side chains of all these residues are exposed to the solvent and are thought to be involved not only in binding the FMN and modulation of reduction potentials, but also in the interaction of Fld with PSI and FNR [6, 31, 32].

Materials and Methods

Biological Materials

Mutations were introduced into the pTrc99a-cloned structural gene encoding the WT Fld from *Anabaena* PCC7119 by using the QuikChange mutagenesis kit (Stratagene) in combination with the following synthetic oligonucleotides (modified bases shown in bold):

5′-CTACGGTACTCAAA**AG**GGTAAAACTGAATCAGTAGCAG- 3' for Thr12 Lys,

5′-CTCAAACTGGTAAAACT**AA**G**T**CAGTAGCAGAAATCATTCG- 3' for Glu16Lys,

5’ -GGCTGTCCTACT**CG****C**AATATTGGCGAACTGCAAAGCG- 3’ for Trp57Arg,

5’-GGCTGTCCTACT**GA**GAATATTGGCGAACTGCAAAGCG- 3’ for Trp57Glu,

5’ -GGCTGTCCTACT**AA**GAATATTGGCGAACTGCAAAGCG- 3’ for Trp57Lys,

5’-GCTTTGCAGTTCGCC**TTC**ATTCCAAGTAGGACAGCC- 3’ for Ile59Glu,

5’-GAAAATTATCTGCGTAACCT**TC**TTGGTCACCAGTCCC- 3’ for Ile92Glu,

5’-GCTTTGCAGTTCGCC**CGC**ATTCCAAGTAGGACAGCC- 3’for Ile59Ala and

5’-GAAAATTATCTGCGTAACCT**GC**TTGGTCACCAGTCCC- 3’ for Ile92Ala.

Double mutants were produced by introducing the second mutation into the single mutant. Mutations were verified by DNA sequence analysis. Fld mutants were over-expressed in *E. coli* and purified as previously reported [33, 34]. The proteins were considered pure when the absorption spectrum showed A_{274}/A_{464} ~ 6.3-6.7 and a single band in SDS-PAGE. ApoFlds were prepared by treating Fld with 3 % trichloroacetic acid at 4 ºC in the presence of dithiothreitol. The precipitated apoprotein was separated from FMN by centrifugation [35], dissolved in 500 mM Tris/HCl pH 8.0 and dialyzed versus 50 mM Tris/HCl pH 8.0.

Spectroscopic analysis

UV/Vis spectra of Flds were recorded on a Cary 300 spectrophotometer. Extinction coefficients of the fully Fld_{ox} forms were determined by FMN release [4], in 50 mM Tris/HCl pH 8.0, using a corrected extinction coefficient of 12.07 mM^{-1} cm^{-1} at 445 nm for free FMN in 50 mM Tris/HCl, pH 8.0, 2% TCA, 0.375 M $NaHCO_3$ [24]. Extinction coefficients for the neutral Fld_{sq} mutants at the maximum around 580 nm were determined from the data obtained during anaerobic photoreduction by plotting absorbance at 580 nm *versus* 464 nm [24]. Extinction coefficients for Thr12Lys, Glu16Lys, Ile59Ala/Ile92Ala and Ile59Glu/Ile92Glu ApoFlds at 278 nm were considered to be the same as that for the WT ApoFld (34.3 mM^{-1} cm^{-1} [34]), but removal of Trp57 was expected to modify this value. To determine the extinction coefficient for the Trp57 ApoFld mutants in 50 mM Tris/HCl, pH 8.0: i) the UV/Vis absorbance spectrum of a 1 ml solution the apoprotein was recorded; ii) this sample was diluted with 7.5 M guanidium hydrochloride in 20 mM phosphate pH 6.5 to 6 M guanidium hydrochloride final concentration; iii) the absorbance spectrum was again recorded. The protein concentration in the diluted solution was calculated using the theoretical extinction coefficient at 280 nm for the denatured apoprotein given by the Expasy ProtParam tool [36]. The initial spectrum and the apoprotein concentration corrected for the dilution were then used to obtain the extinction coefficient in 50 mM Tris/HCl, pH 8.0. Fluorescence emission spectra in the visible region (from 500 to 600 nm, excitation at 445 nm) were recorded in an Aminco-Bowman Series 2 spectrofluorimeter in 50 mM Tris/HCl, pH 8.0 at 25 ºC. Circular dichroism spectra were recorded in a Chirascan spectropolarimeter (Applied Photophysics Ltd.), in 1 mM Tris/HCl, pH 8.0 at 25 ºC with 20 μM protein. Cuvettes of path length 0.1 cm were used for the far-UV, and of 0.4 cm for the near UV/Vis regions.

Reduction Potential Determinations.

Midpoint reduction potentials of the ox/sq and sq/hq couples were determined at 25ºC in 50 mM Tris/HCl pH 8.0, by anaerobic photoreduction using a gold electrode and a saturated calomel electrode as reference [24, 37]. The midpoint potentials are reported relative to the potential of the standard hydrogen electrode. The experimental solutions contained 25-100 μM protein, 1 mM EDTA, 1-2 μM deazariboflavin and 1 μM indicator dyes at 25 °C. They were irradiated with light from a 250 W slide projector for different periods of time to reduce the protein stepwise. Equilibration of the system was considered established when the potential, measured with a Sycopel Ministat potentiostat, remained stable for 20 min. The UV-Vis spectrum was then recorded in a Cary 300 spectrophotometer. The concentrations of the different redox species at equilibrium were determined from the absorbance spectra. The two one-electron steps in reduction could be analyzed separately because only ox and sq states were present during most of the first step and only sq and hq were present during most of the second. The concentration of sq was calculated from the absorbance of the 580 nm band, and the concentration of the other species was determined by subtraction of the sq from the total concentration of Fld. The midpoint potentials for the redox couples were calculated by linear regression according to the Nernst equation.

$$E = E_m + (0.059/n) \log ([ox]/[rd]) \qquad [1]$$

The following dyes were used as mediators: anthraquinone-2,6-disulfonate ($E_{m,pH7}$= -184 mV) and anthraquinone-2-sulfonate ($E_{m,pH7}$= -225 mV) for the determination of $E_{ox/sq}$ and benzyl viologen ($E_{m,pH7}$= -359 mV) and methyl viologen ($E_{m,pH7}$= -446 mV) for the determination of $E_{sq/hq}$. Error in the $E_{ox/sq}$ and $E_{sq/hq}$ determined was estimated to be ± 5 mV.

Dissociation Constants

Dissociation constants (K_d) for the ApoFld:FMN_{ox} complexes were determined by quenching of the FMN fluorescence upon ApoFld titration at 25ºC. In a typical experiment, 1 ml of 0.2 μM FMN (98% pure, SIGMA) in 50 mM Tris/HCl, pH 8.0, was titrated with aliquots of a 5-17 μM ApoFld solution. After each addition the system was allowed to equilibrate for 2 min. Excitation was at 445 nm and emission was monitored at 525 nm. The fluorescence emission was fit to equation [2] to calculate K_d [9]:

$$F=F_{end} + F_{\delta} (dC_F - [(C_A + K_d + dC_F) - [(C_A + K_d + dC_F)^2 - 4C_A dC_F]^{1/2}]/2) \qquad [2]$$

where F is the observed emission intensity after each addition, F_{end} the remaining emission intensity at the end of the titration, F_{δ} the difference in emission intensity between 1 μM free flavin and 1 μM Fld, C_A the total protein concentration after each addition, C_F the starting concentration of flavin (considered as unknown), and d the dilution factor of this initial concentration after each addition. In all cases C_F was correctly predicted by the fitting (within ± 5%). Error in K_d values was estimated ±10%.

Free energy calculation

The reduction potentials of ApoFld:FMN complexes are linked to the binding affinities of the different FMN redox forms (Figure 2A) [9, 38]. Thus, the free energies for the ApoFld:FMN_{sq} (ΔG_{sq}) and ApoFld:FMN_{hq} (ΔG_{hq}) complexes can be calculated from the following equations:

$$\Delta G_{sq} = \Delta G_{ox} - F(E_{ox/sq} - E_{ox/sq}^{free}) \qquad [3]$$

$$\Delta G_{hq} = \Delta G_{ox} - F(E_{ox/sq} + E_{sq/hq} - E_{ox/sq}^{free} - E_{sq/hq}^{free}) \qquad [4]$$

where F is the Faraday constant and $E_{ox/sq}^{free}$ and $E_{sq/hq}^{free}$, the midpoint reduction potentials for free FMN. E_m^{free} was calculated by fitting the reported experimental values at different pH values [39] to equation 3 from [40]. $E_{ox/sq}^{free}$ at pH 8.0 was

obtained using equation 5 in [40] that fits experimental data from [41]. $E_{sq/hq}^{free}$ was derived using equation 4 from [40]. SD in the determined ΔG values was ±0.5.

Crystal growth, data collection, and structure refinement

Trp57Glu and Ile92Ala Fld variants were crystallized using the hanging-drop vapour-diffusion method at 293K. The search of initial crystallization conditions was carried out using the *Jena-Bioscience* screens Basic 1, Basic 2, Basic 3 and Basic 4. The conditions yielding crystals were further optimized. Final Trp57Glu and Ile92Ala crystals grew in 4 μl droplets containing 2 μl of 10 mg ml^{-1} protein solution buffered with 10 mM Tris/HCl, pH 8.0 and 2 μl of reservoir solution. Droplets, were equilibrated against 0.5 ml of reservoir solution which consisted of 0.1M Tris/HCl, pH 8.5 and 0.2 M $MgCl_2$, with 32% PEG 4000 for Ile92Ala and 28% PEG 4000 for Trp57Glu. Ile92Ala crystals grew within 1-7 days and those of Trp57Glu did within 2-4 weeks.

X-ray diffraction data sets for crystals of the Trp57Glu variant were measured using an Enraf-Nonius rotating anode generator and collected on a Mar Research image-plate detector. X-ray diffraction data sets for crystals of the Ile92Ala variant were measured using a graphite-monochromated CuK_α radiation generated by a Microstar-micro focus rotating anode collected on a CCD detector. In both cases crystals were frozen under a liquid nitrogen stream at 100K. Trp57Glu crystals belong to the monoclinic $P2_1$ space group (*a*=37.85 Å, *b*=55.58 Å, *c*=70.26 Å, β=91.17º) and those of Ile92Ala to the monoclinic C2 space group (*a*=110.96 Å, *b*=37.49 Å, *c*=90.60 Å, β=123.66) (see Table 1). Calculated Matthews coefficients for Ile92Ala and Trp57Glu estimated the presence of two molecules in the asymmetric unit and 41.08 % and 36.26 % of solvent content respectively (V_M=2.09 $Å^3$ Da^{-1} and 1.94 $Å^3$ Da^{-1} for Ile92Ala and Trp57Glu, respectively). X-ray data set for Trp57Glu diffracts up to 1.88 Å resolution and was processed and scaled using the programs MOSFLM [42] and SCALA from the

CCP4 package [43]. X-ray data set for Ile92Ala diffracts up to 1.99 Å resolution and was processed and scaled using the programs SAINT and SADABS from the Proteum2 software suite (Bruker AXS Inc., 2006).

The structures of Trp57Glu and Ile92Ala Flds were solved by the molecular replacement method on the bases of the structure of the oxidized WT and Trp57Leu Flds from *Anabaena* (PDB codes 1flv and 1obo, respectively) [7] and using the program MOLREP [44]. In both cases, unambiguous and single solutions for the rotation and translation functions were obtained. Structure refinement was performed using the programs CNS [45], and REFMAC5 [46]. This process was alternated with manual model building using the software package O [47]. The quality of the final models was checked using the program PROCHECK [48]. All residues in the Ramachandran plot fall within the allowed regions. Crystallographic data and statistics of the models are summarized in Table I. The final structure of Trp57Glu Fld contains two independent protein molecules in the asymmetric unit, two FMN molecules, one Mg^{2+}, and 240 water molecules. The final model for Ile92Ala Fld contains two protein molecules in the asymmetric unit, two FMN molecules, and 198 water molecules. Pictures were generated with PyMol [49]. Atomic coordinates and structure factors for Fld variants have been deposited in the PDB with accession codes 2v5v for Trp57Glu Fld, and 2v5u for Ile92Ala Fld.

Structural models for Fld mutants

In silico mutations were performed on the three-dimensional structure of WT *Anabaena* Fld_{ox} (PDB accession code: 1flv) using the mutation tool implemented in Swiss-Pdb Viewer [50]. Subsequent energy minimization was done using the AMBER package of molecular dynamics simulations [51]. The WT and all the models were protonated and for the FMN_{ox} a set of force-field parameters previously reported was

used [52]. The minimization was performed with 1000 steps of Steepest Descent and 2000 steps of Conjugate Gradient. The validity of the method was assessed by treating in the same way the X-ray structures reported for *Anabaena* WT and Trp57Leu Flds [5, 7] as well as those obtained for Trp57Glu and Ile92Ala in the present work. The r.m.s.d. for all atoms of molecules modeled with regard to the corresponding crystallographic structures was under 0.2 Å for backbone atoms. Additionally, comparison of flavin surface accessible to the solvent between crystallographic structures for the WT, Trp57Glu and Trp57Leu Flds resulted in similar values. The external FMN (or flavin ring) solvent accessible surface and the contacts in the minimized proteins were calculated using the Ligand-Protein Contacts software (http://bip.weizmann.ac.il/oca-bin/lpccsu/) [53].

Results

Expression, purification and spectral properties of the Fld Mutants

The levels of expression of all the mutants and their general circular dichroism spectral properties in the UV regions were similar to those of the WT Fld (not shown), indicating that the mutated proteins fold and bind FMN without major structural perturbations with regard to WT Fld. Although the overall shapes of the absorbance spectra were similar, some of the mutants, in particular those for Trp57, differed in the positions of the visible maxima as well as in their extinction coefficients (Figure 1A, Table 2). Thus, replacement of Trp57 by an amino acid with either a positively or negatively charged side chain caused the absorption maxima (band I at 463 nm; band II at 374 nm in WT) to be blue-shifted relative to WT. This displacement was up to 7 nm in the case of band I for the Trp57Glu and Trp57Arg mutants (Table 2). The changes suggested that replacement of Trp57 by Glu, Lys or Arg modified the close environment of the flavin ring. In general, the extinction coefficients of band I differed only slightly from that of the WT Fld, and changes were measurable only with the Trp57 and the Ile59Glu/Ile92Glu mutants (Table 2). These observations are consistent with a more polar environment in those mutants. Removal of Trp57 decreased the extinction coefficient of the ApoFld in the UV region from 34.3 mM^{-1} cm^{-1} to 30.5 mM^{-1} cm^{-1} at the 277 nm maximum.

All of the mutants stabilized the blue neutral sq upon partial reduction. The positions of the absorbance maxima of the sq long-wavelength band for the Trp57 mutants, as well as the isosbestic point for the ox/sq transitions, were again blue-shifted compared to WT Fld (Table 2). Smaller extinction coefficients for the sq forms of Trp57Arg and the two double mutants were also observed (Table 2). Finally, the extent

of sq stabilization at half reduction decreased for the two double mutants (~60% for Ile59Ala/Ile92Ala and ~82% for Ile59Glu/Ile92Glu *versus* ~97% for WT Fld).

Replacement of Trp57, a residue in contact with the isoalloxazine ring, by Glu, Lys or Arg, resulted in a 10-fold increase of the quantum yield of fluorescence (2.9%, 4.6% and 3.6% of free FMN fluorescence respectively). A similar increase in fluorescence emission was observed when Thr12 was replaced by Lys (2.7%). The decreased quenching of FMN fluorescence in these mutants with regard to WT Fld (only 0.3% of that of free FMN [9]) suggests that their FMN molecules may be more exposed to solvent than in WT Fld.

Reduction potentials

Differences from WT Fld were observed in the reduction potentials determined from the Nernst plots of the two one-electron processes at pH 8.0 and 25 ºC for the mutants (Figure 1, Table 3). Although both midpoint reduction potentials, $E_{ox/sq}$ and $E_{sq/hq}$, were altered for most of the mutants, much larger differences were found for $E_{ox/sq}$ (ΔE from -71 to +78 mV) than for $E_{sq/hq}$ (ΔE from -1 to +49 mV).

Introduction of a positively-charged amino acid, Lys, in place of either Thr12 or Glu16 produced relatively small effects on $E_{ox/sq}$ (+12 and +14 mV, respectively), and no effect on $E_{sq/hq}$ (Table 3, Figures 1C and 1D). Replacement of Trp57 by either a positively (Lys or Arg) or a negatively (Glu) charged residue caused both $E_{ox/sq}$ and $E_{sq/hq}$ to be considerably less negative (Table 3, Figures 1C and 1D). These changes in the two values led to only a small decrease in stability of the sq in these mutants. Moreover, it is notable that the change in $E_{ox/sq}$ for the Trp57Lys mutant is large (+78 mV compared with +28 mV for $E_{sq/hq}$), while the relative sizes of the changes are reversed when Trp57 is replaced by either Arg or Glu (Table 3). The two double mutants at Ile52 and Ile92, especially when both Ile residues were simultaneously

replaced by Ala (Figure 1B), were the species showing the greatest effects (Table 3, Figures 1C and 1D). For these mutants, the reduction potentials for the two 1-electron steps converged, causing the percentage of sq stabilized at half reduction to decrease. Thus, simultaneous replacement of both Ile residues by Ala made $E_{ox/sq}$ 71 mV more negative and $E_{sq/hq}$ 48 mV less negative, while the simultaneous replacement of these residues by Glu made $E_{ox/sq}$ 52 mV more negative and $E_{sq/hq}$ only 17 mV less negative.

Dissociation constants

K_d values for the ApoFld:FMN_{ox} complexes were determined by measuring the quenching of FMN fluorescence in titration experiments with ApoFld (Table 4). The affinity of Glu16Lys ApoFld was found to be similar to that of WT, while slightly weaker complexes (0.6 – 1.3 Kcal/mol) were formed with the rest of the mutants. Free energy data for the interaction indicated that the sq complex for WT Fld was slightly more stable than the ox complex, while reduction to the hq considerably destabilized the flavin-protein interaction (Table 4) [9, 24]. The energy profile for the Glu16Lys mutant was almost identical to that of WT, and the profile for the Thr12Lys mutant was similarly displaced for all the states (Figure 2B). Thus, while Glu16 is apparently not implicated in FMN binding and stabilization, a Lys at position 12 produced a similar weakening of FMN binding in all redox states of the cofactor. Simultaneous replacement of Ile59 and Ile92 by either Ala or Glu clearly modified the binding profile (Figure 2B). The mutations decreased the affinity of ApoFld for FMN in all three redox states, but the effect was much more pronounced when the flavin was reduced, and particularly when it was present as the sq. Finally, replacement of Trp57 produced different effects depending on the residue introduced (Figure 2C). Thus, introduction of a Glu made both the ox and sq complexes slightly more unstable, but the FMN_{hq} affinity was almost unchanged. Replacement of Trp57 by a positively charged side chain, either

Arg or Lys, produced considerable destabilization of ApoFld:FMN_{ox}, while the stability of ApoFld:FMN_{hq} increased. However, when Lys or Arg was substituted for Trp57 opposite effects were produced in the stability of the ApoFld:FMN_{sq} complex (Figure 2C). In Trp57Lys the sq was more stable than in WT, whereas in Trp57Arg it was slightly less stable (Table 4).

Crystal structure of the Trp57Glu and Ile92Ala Anabaena Fld variants

The three-dimensional structures of the Trp57Glu and Ile92Ala Fld variants were solved by the molecular replacement methods and refined up to 1.88 and 1.99 Å resolution, respectively. The overall folding of these Fld variants showed no significant differences with respect to the native Fld, as shown by the r.m.s.d. of the Cα backbones (0.37 Å and 0.24 Å for the Trp57Glu and Ile92Ala Fld variants, respectively). Larger differences in the overall backbone were only found in the 26-29 and 132-138 loops, regions where high flexibility is found when comparing different Flds, particularly the second loop that corresponds to the extra region in "long-chain" Flds [7]. In the Trp57Glu variant structure, the Glu57 side chain was not oriented toward the ribityl moiety of FMN, as occurs with Trp57 in WT, being rather projected to the protein surface (Figure 3). Replacement of Trp57 with Glu also disturbed a number of interactions between Trp57 and the FMN, particularly the stacking interaction with the flavin ring (Figures 3 and 4). The position of the side chain of Glu57 resulted stabilized by an ordered H-bond network formed between water molecules and several residues of the environment. Particularly, one of the oxygens of the Glu57 carboxylate group was stabilized by forming a water mediated H-bond with the PO2 moiety of FMN (Figures 3 and 4). The water molecule mediating this bridge is not present in WT Fld, is mimicking the role of the NE1 indol of Trp57 in WT Fld and also preventing the repulsion between the FMN phosphate group and the negatively charged carboxylate

group of Glu57. Noticeably, a water molecule is also found stabilizing the FMN phosphate group in the structure reported for the *Anabaena* Trp57Leu Fld variant [5], although in this case the Leu side chain can not contribute to H-bond the water molecule (Figure 3). In both, Trp57Leu and, particularly, Trp57Glu, reorganization of this H-bond around the phosphate group of FMN resulted in a slight displacement of the position of the phosphate, ribityl and flavin ring moieties of FMN with regard to the position found in WT Fld (Figure 4A). The fact that the smaller Glu side chain resulted stabilized far away from the flavin ring enlarged the FMN binding site, increased the exposure to the solvent of the isoalloxazine ring and altered the electrostatic surface potential around the flavin binding site (Figure 3).

The Ile92Ala conservative mutation did not produce major alterations in the Fld structure. However, analysis of the close environment of the flavin ring indicated that the distance between the N5 of the flavin and the N-Ile59 was of only 3.24 Å, versus the 3.7 Å reported in WT Fld (1flv, [7] Figure 4B). Such distance was similarly decreased to 3.4 Å in the three-dimensional structures of Trp57Glu and Trp57Leu Flds. These observations further support the existence of the H-bond interaction, N5-HN-Ile59, in the FMN oxidized state of *Anabaena* Fld. Such interaction was suggested when the WT Fld structure was first reported, despite the measured distance, 3.7 Å, was slightly beyond that expected for a H-bond [7]. It is worth to notice that in the particular case of Trp57Glu, the shorter H-bond distance would provide a stronger interaction between the flavin and the apoprotein. However, as above mentioned, the mutation also disturbed a number of interactions between Trp57 and the FMN, conciliating with the slighter weaker FMN binding observed for this mutant. Comparative observation of all the structures so far reported for *Anabaena* Fld variants also indicates: i) slight displacements of the stacking positions of Trp57 and Tyr94 with regard to the oxidized

flavin ring, which suggest some dynamics for this positions, ii), the ability of Lys14 side chain to adopt different conformations and interactions on the protein surface that produce different accessibility to the solvent of the ribityl, as well as differences in the surface electrostatic potential around this area.

Discussion

The phosphate binding loop residues. A Lys residue in place of either Thr12 or Glu16 Fld produced small effects on $E_{ox/sq}$ or $E_{sq/hq}$ (Table 3), as reported for the introduction of a His in this loop of *D. vulgaris* Fld [54]. Moreover, no major effects were detected for the interaction of Glu16Lys ApoFld with FMN (Figure 2B, Table 4). Glu16 side chain is not interacting with FMN, suggesting a similar situation for Lys16 and indicating that this side chain does not modulate FMN binding. However, a Lys residue at Thr12 weakened the ApoFld:FMN_{ox}, ApoFld:FMN_{sq} and ApoFld:FMN_{hq} interactions (Table 4). Comparison of the WT structure with a Thr12Lys Fld model suggests the lack of a H-bond between the Lys12 and the phosphate as the main responsible for the weakening of this interaction (not shown).

Trp57 and the 50´s loop. Placing Arg or especially Lys at position 57 in *Anabaena* Fld facilitates reduction to the Fld_{sq}, whereas a Glu has a more moderate effect (Table 3). The effect of introducing Arg is similar to that reported for the introduction of an Ala, a Lys produced similar effects than a Phe and, especially, a Tyr, and a Glu produces a $E_{ox/sq}$ more similar to those of Trp57Leu and WT Flds [9]. Trp57 establishes several interactions to stabilize the ApoFld:FMN complex. These include a H-bond to the phosphate group, aromatic-aromatic interactions with the pyrazine and benzyl moieties of the flavin, and apolar-apolar and apolar-polar contacts with the ribityl, phosphate, pyrazine and benzyl portions of FMN. Positions of Glu57 or Leu57 in the crystal structures of Trp57Glu and Trp57Leu Flds suggest that despite substitution of Trp by Leu, Glu, Lys or Arg removes the flavin:Trp aromatic interaction, the main polar-polar interactions that bind the FMN group in its cavity are unaffected. Thus, the only H-bond provided by the Trp side chain in WT Fld is provided by a water molecule in the case of the Trp57Glu and the Trp57Leu structures. Moreover, in the

particular case of Trp57Glu this water molecule simultaneously stabilizes the position of the PO2 group of FMN and that of the new carboxylate towards the protein surface (Figures 3 and 4). These observations are in agreement with these mutants presenting only slightly weaker ApoFld:FMN_{ox} interactions than WT Fld (Figure 2C, Table 4). The X-ray structures for the Trp57Glu and Trp57Leu mutants also showed that the mutations enlarged the FMN cavity, increasing the flavin ring accessibility to the solvent and altering the protein electrostatic surface around the FMN binding site with regard to WT Fld (Figure 3). Changes in the flavin solvent accessibility and electrostatic potential will be expected also for the rest of the mutants, as supported by their *in silico* models (not shown). However, there is no correlation between flavin solvent accessibility and $E_{ox/sq}$ (Figure 5A), in agreement with the fact that not water molecules have been shown to occupy the cavity left by the Trp around the flavin ring in the structure of Trp57Glu (Figure 3). Therefore, the side chain at position 57 does not contribute to set $E_{ox/sq}$ neither by placing an aromatic side chain adjacent to the flavin ring nor by excluding the flavin ring from the solvent. Moreover, similar effects are produced by side chains with different properties, the shorter side chains resembling more the WT Trp behavior. The different effects found with Trp and Tyr agree with solution studies suggesting that whereas Tyr shows a strong affinity for the flavin sq and almost no affinity for the ox, Trp preferentially stabilizes the ox state and thermodynamically destabilizes the flavin sq [55]. The Trp57Glu structure also shows that the mutation produces a displacement of the flavin ring towards the 50´s loop that affects the N(5)-HN59 H-bond distance (Figure 4), which surely will affect the N(5)H-OC58 distance in the sq state. The more positive values for the $E_{ox/sq}$ of the Trp57Lys and Trp57Arg mutants and their weaker affinities for FMN_{ox} are consistent with the more favorable thermodynamic conversion to the sq (Tables 3 and 4). This would be

explained if the distance between N(5) and HN59 increases in these mutants, thus decreasing the conformational energy of the Asn58-Ile59 peptide bond and favoring the "O-up" conformation. Despite the absence of X-ray structures for these mutants, *in silico* models and weaker ApoFld:FMN_{ox} parameters support the increase of these H-bond distances. Therefore, the nature of the residue at position of Trp57 appears to influence the "O-down to O-up" conformational change at the Asn58-Ile59 peptide bond on one electron-reduction of Fld_{ox}, making reduction more or less difficult and shifting $E_{ox/sq}$ to more or less negative values [3, 19].

The sq forms of the mutants in which Trp57 was replaced by Glu, Lys and especially Arg are also easier to reduce to the hq (Table 3), confirming that the nature of the side chain at this position also contributes to the modulation of $E_{sq/hq}$ [9]. Optical properties indicate that the solvent accessibility of the flavin has increased in these mutants (Table 2). This is also consistent with the enlargement observed in the FMN cavity in the X-ray structure of Trp57Glu (Figure 3) that would allow a FMN_{hq} butterfly bending. This putative bending will be in agreement with stabilization of the hq state, in contrast with the coplanar interactions with aromatic side chains present in the WT Fld that enforce flavin planarity and account for hq destabilization [56]. The plot of $E_{sq/hq}$ values reported to date for different Fld mutants [9, 24] *versus* the isoalloxazine solvent accessible surface of the oxidized state displays two different effects (Figure 5B). In a large group of mutants the solvent accessible surface is not changed (despite changes in $E_{sq/hq}$), while in mutants at the positions stacking the flavin ring, Tyr94 and Trp57, there is a clear correlation. The FMN exposure increase correlates with generally less negative $E_{sq/hq}$ (Figure 5B), suggesting than in the hq state solvent molecules might solvate the anionic flavin ring. $E_{sq/hq}$ would undoubtedly be also modulated by other factors. FMN_{hq} in Flds exists as the anion, being its formation

energetically unfavorable in the apolar apoprotein environment [3, 57]. Moreover, the negative charge on the flavin, at N(1), is in a protein environment characterized by the presence of several negatively-charged side chains [10, 15, 58, 59]. These effects also contribute to the very low $E_{sq/hq}$ in Flds, and changes in the polarity and the electrostatic properties of the flavin environment modulate it [15, 57, 58, 60]. Therefore, the more electron-rich aromatic side chains are expected to produce more negative values [9] and, the introduction of charged residues modifies both the electrostatics and the polarity of the isoalloxazine environment. The introduction of a Glu57 side chain in Fld thermodynamically stabilized the hq state (Table 3). Addition of a negative charge in the close environment of the FMN would not be expected to favor the hq formation, however, the increase in FMN solvent accessibility appears to offset the effect of the charge. Replacement of Trp57 by Lys or Arg, shifts $E_{sq/hq}$ to less negative values, correlating with the increase in FMN solvent accessible surface (Figure 5B) and with the possibility of a stacking cation-π stabilizing interaction between the introduced positive side chain and electron density rich flavin hq ring. This later observation is also in agreement with the stabilization shown for the ApoFld:FMN_{hq} binding (Table 4).

The hydrophobic residues at the 50's and 90`s loops. Replacement of Ile59 and Ile92 with Glu, and especially Ala, makes reduction to the sq state considerably less favorable by shifting $E_{ox/sq}$ close to that of free FMN, whereas $E_{sq/hq}$ shifted to less negative values (Table 3). Therefore, the ox/sq conversion results hindered while the sq/hq one is favored by comparison with WT and an important increase in the energy required for the "O-down to O-up" conformational change appears to apply in this particular mutants. These changes in reduction potentials also correlate with a decrease in the affinity of the ApoFld forms of these mutants for all the redox states of FMN (Figure 2B). The structure of a mutant containing the single Ile92Ala mutation

indicates only minor overall structural changes, suggesting mutations at Ile59 must mainly modulate binding affinities and reduction potentials. Models of the double mutants indicate the side chain at position 59 will be projected to the solvent, suggesting that the introduced mutations will hardly affect the contact surface between FMN_{ox} and position 59. However, different side chains at this position will modulate the relative orientation and distance of the atoms producing the N(5)–NH59 H-bond either in the ox or hq states (Figure 4B). Conversely, the conformational change expected upon conversion to the sq state and the corresponding N(5)–OC58 H-bond expected to be formed in this state would be also affected. This later observation is fully consistent with these mutants presenting a weaker FMN binding affinity, especially for FMN_{sq} (Figure 2B). Unfortunately, no three dimensional structures for mutants at position Ile59 have been so far obtained.

The structure reported for the *A. nidulans* WT Fld_{hq} shows that the Asn58-Val59 peptide (Asn58-Ile59 in *Anabaena* Fld) exhibits the "O-down" conformation characteristic of the Fld_{ox} [26]. Such reversion to the "O-down" conformation from the "O-up" found in the Fld_{sq} upon reduction to the Fld_{hq} state has not been observed in other Flds [3, 19]. However, since the redox and structural properties of *Anabaena* and *A. nidulans* Flds follow similar patterns, such structural rearrangement might be also expected in *Anabaena* Fld_{hq}. $E_{ox/sq}$ data suggest that reorientation of the Asn58-Ile59 peptide from the ox to the sq state to form the N(5)H-OC58 H-bond appears to be hindered in the Ile59Ala/Ile92Ala and Ile59Glu/Ile92Glu double mutants (Table 3). Thus, if the structure of their Fld_{hq} state resembles that of *A. nidulans* Fld, it would be expected that conversion from the sq to the hq state will be favored, since it will be accompanied by reversion to the "O-down" conformation which appears a more preferred state for these mutants compared to WT. This is consistent with: i) a greater

relative weakening in the FMN_{hq}, and especially FMN_{sq}, interactions with regard to FMN_{ox} (Figure 2B) and, ii) destabilization of Fld_{sq} formation and stabilization of Fld_{hq} formation (Table 3). This confirms the importance of N(5) and N(5)H H-bonds with Asn58 and Ile59, respectively, and is consistent with the energies related to the conformational changes occurring in the Ans58-Ile59 backbone upon forming the sq state as major contributors to the modulation of reduction potentials [24]. Additionally, replacement of the neutral Ile59 and Ile92 side chains with acidic residues in the 50's and 90´s loops might also affect the sq/hq equilibrium, generally making $E_{sq/hq}$ more negative [26]. This is reflected by simultaneous replacement of Ile59 and Ile92 with Glu that shifted $E_{sq/hq}$ to less positive values than when introducing Ala.

The data here presented indicate that side chains of the P-binding loop of *Anabaena* Fld function in FMN binding rather that in determining the FMN reduction potentials. The side chain of Trp57 both modulates the FMN binding profile and helps to establish the low $E_{sq/hq}$ by stacking the flavin within the protein and preventing the flavin bending. This ensures that the flavin is in an electronegative environment that allows tight FMN_{hq} binding while making formation of its anion thermodynamically unfavorable. Nevertheless, in *Anabaena* Fld the aromatic character of Trp57 must have a relatively minor contribution because all the mutants still have the very low value for $E_{sq/hq}$ that typifies the Fld family [9, 57]. Thus, in this particular case, Trp57 contributes to the modulation of $E_{ox/sq}$ by helping to orientate the flavin with regard to the Asn58-Ile59 peptide bond. Finally, the side chain at position 59 in *Anabaena* Fld contributes to the strength of FMN binding, especially for FMN_{sq}, and therefore contributes to modulate both $E_{ox/sq}$ and $E_{sq/hq}$. The nature of the residue in this position contributes to modulate the Asn58-Ile59 peptide ability to H-bond with the N(5) or N(5)H position of

FMN and to the energy of the conformational change of this peptide bond upon FMN reduction, thus modulating the equilibrium of the "O-dowm to O-up" conversion.

Acknowledgements: This work has been supported by Grants BIO2004-00279 and PIP122/2005 to M.M.. We thank to C. Hamiaux and B. Schierbeek from Bruker for collecting and partially processing the X-ray data for the Ile92Ala Fld.

REFERENCES

[1] S.G. Mayhew, M.L. Ludwig, Flavodoxins and electron-transferring flavoproteins, Enzymes 12 (1975) 57.

[2] S.G. Mayhew, G. Tollin, General properties of Flavodoxins, in: F. Müller (Ed.), Chemistry and Biochemistry of Flavoenzymes, CRC Press, Boca Raton, Florida, 1992, pp. 389-426.

[3] M.L. Ludwig, K.A. Pattridge, A.L. Metzger, M.M. Dixon, M. Eren, Y. Feng, R.P. Swenson, Control of oxidation-reduction potentials in flavodoxin from *Clostridium beijerinckii*: the role of conformation changes, Biochemistry 36 (1997) 1259-1280.

[4] S.G. Mayhew, G.P. Foust, V. Massey, Oxidation-reduction properties of flavodoxin from *Peptostreptococcus elsdenii*, J Biol Chem 244 (1969) 803-810.

[5] A. Lostao, F. Daoudi, M.P. Irun, A. Ramon, C. Fernandez-Cabrera, A. Romero, J. Sancho, How FMN binds to *Anabaena* apoflavodoxin: a hydrophobic encounter at an open binding site, J Biol Chem 278 (2003) 24053-24061.

[6] A. Lostao, M. El Harrous, F. Daoudi, A. Romero, A. Parody-Morreale, J. Sancho, Dissecting the energetics of the apoflavodoxin-FMN complex, J Biol Chem 275 (2000) 9518-9526.

[7] S.T. Rao, F. Shaffie, C. Yu, K.A. Satyshur, B.J. Stockman, J.L. Markley, M. Sundarlingam, Structure of the oxidized long-chain flavodoxin from *Anabaena* 7120 at 2 A resolution, Protein Sci 1 (1992) 1413-1427.

[8] M.L. Ludwig, C.L. Luschinsky, Structure and redox properties of clostridial flavodoxin. , in: F. Müller (Ed.), Chemistry and Biochemistry of Flavoenzymes, CRC Press, Boca Raton, Fl., 1992, pp. 427-466.

[9] A. Lostao, C. Gomez-Moreno, S.G. Mayhew, J. Sancho, Differential stabilization of the three FMN redox forms by tyrosine 94 and tryptophan 57 in flavodoxin from *Anabaena* and its influence on the redox potentials, Biochemistry 36 (1997) 14334-14344.

[10] L.H. Bradley, R.P. Swenson, Role of glutamate-59 hydrogen bonded to N(3)H of the flavin mononucleotide cofactor in the modulation of the redox potentials of the *Clostridium beijerinckii* flavodoxin. Glutamate-59 is not responsible for the pH dependency but contributes to the stabilization of the flavin semiquinone, Biochemistry 38 (1999) 12377-12386.

[11] L.H. Bradley, R.P. Swenson, Role of hydrogen bonding interactions to N(3)H of the flavin mononucleotide cofactor in the modulation of the redox potentials of the *Clostridium beijerinckii* flavodoxin, Biochemistry 40 (2001) 8686-8695.

[12] F. Chang, L.H. Bradley, R.P. Swenson, Evaluation of the hydrogen bonding interactions and their effects on the oxidation-reduction potentials for the riboflavin complex of the *Desulfovibrio vulgaris* flavodoxin, Biochim Biophys Acta 1504 (2001) 319-328.

[13] F.C. Chang, R.P. Swenson, Regulation of oxidation-reduction potentials through redox-linked ionization in the Y98H mutant of the *Desulfovibrio vulgaris* [Hildenborough] flavodoxin: direct proton nuclear magnetic resonance spectroscopic evidence for the redox-dependent shift in the pKa of Histidine-98, Biochemistry 36 (1997) 9013-9021.

[14] L.J. Druhan, R.P. Swenson, Role of methionine 56 in the control of the oxidation-reduction potentials of the *Clostridium beijerinckii* flavodoxin: effects of substitutions by aliphatic amino acids and evidence for a role of sulfur-flavin interactions, Biochemistry 37 (1998) 9668-9678.

[15] A.A. McCarthy, M.A. Walsh, C.S. Verma, D.P. O'Connell, M. Reinhold, G.N. Yalloway, D. D'Arcy, T.M. Higgins, G. Voordouw, S.G. Mayhew, Crystallographic investigation of the role of aspartate 95 in the modulation of the redox potentials of *Desulfovibrio vulgaris* flavodoxin, Biochemistry 41 (2002) 10950-10962.

[16] V. Massey, The chemical and biological versatility of riboflavin, Biochem Soc Trans 28 (2000) 283-296.

[17] V. Massey, G. Palmer, On the existence of spectrally distinct classes of flavoprotein semiquinones. A new method for the quantitative production of flavoprotein semiquinones, Biochemistry 5 (1966) 3181-3189.

[18] D.M. Hoover, M.L. Ludwig, A flavodoxin that is required for enzyme activation: the structure of oxidized flavodoxin from *Escherichia coli* at 1.8 A resolution, Protein Sci 6 (1997) 2525-2537.

[19] W. Watt, A. Tulinsky, R.P. Swenson, K.D. Watenpaugh, Comparison of the crystal structures of a flavodoxin in its three oxidation states at cryogenic temperatures, J Mol Biol 218 (1991) 195-208.

[20] J. Freigang, K. Diederichs, K.P. Schafer, W. Welte, R. Paul, Crystal structure of oxidized flavodoxin, an essential protein in *Helicobacter pylori*, Protein Sci 11 (2002) 253-261.

[21] S. Alagaratnam, G. van Pouderoyen, T. Pijning, B.W. Dijkstra, D. Cavazzini, G.L. Rossi, W.M. Van Dongen, C.P. van Mierlo, W.J. van Berkel, G.W. Canters, A crystallographic study of Cys69Ala flavodoxin II from *Azotobacter vinelandii*: structural determinants of redox potential, Protein Sci 14 (2005) 2284-2295.

[22] M.H. Drummond, The base sequence of the nifF gene of *Klebsiella pneumoniae* and homology of the predicted amino acid sequence of its protein product to other flavodoxins, Biochem J 232 (1985) 891-896.

[23] Y. Hu, Y. Li, X. Zhang, X. Guo, B. Xia, C. Jin, Solution structures and backbone dynamics of a flavodoxin mioC from *Escherichia coli* in both apo- and holo- forms: Implications for cofactor binding and electron transfer, J Biol Chem (2006).

[24] I. Nogues, L.A. Campos, J. Sancho, C. Gomez-Moreno, S.G. Mayhew, M. Medina, Role of neighboring FMN side chains in the modulation of flavin reduction potentials and in the energetics of the FMN:apoprotein interaction in *Anabaena* flavodoxin, Biochemistry 43 (2004) 15111-15121.

[25] A. Romero, J. Caldeira, J. Legall, I. Moura, J.J. Moura, M.J. Romao, Crystal structure of flavodoxin from *Desulfovibrio desulfuricans* ATCC 27774 in two oxidation states, Eur J Biochem 239 (1996) 190-196.

[26] D.M. Hoover, C.L. Drennan, A.L. Metzger, C. Osborne, C.H. Weber, K.A. Pattridge, M.L. Ludwig, Comparisons of wild-type and mutant flavodoxins from *Anacystis nidulans*. Structural determinants of the redox potentials, J Mol Biol 294 (1999) 725-743.

[27] M. Kasim, R.P. Swenson, Alanine-scanning of the 50's loop in the *Clostridium beijerinckii* flavodoxin: evaluation of additivity and the importance of interactions provided by the main chain in the modulation of the oxidation-reduction potentials, Biochemistry 40 (2001) 13548-13555.

[28] F.C. Chang, R.P. Swenson, The midpoint potentials for the oxidized-semiquinone couple for Gly57 mutants of the *Clostridium beijerinckii* flavodoxin correlate with changes in the hydrogen-bonding interaction with the proton on N(5) of the reduced flavin mononucleotide cofactor as measured by NMR chemical shift temperature dependencies, Biochemistry 38 (1999) 7168-7176.

[29] I. Nogues, M. Martinez-Julvez, J.A. Navarro, M. Hervas, L. Armenteros, M.A. de la Rosa, T.B. Brodie, J.K. Hurley, G. Tollin, C. Gomez-Moreno, M. Medina, Role of hydrophobic interactions in the flavodoxin mediated electron transfer from photosystem I to ferredoxin-$NADP^+$ reductase in *Anabaena* PCC 7119, Biochemistry 42 (2003) 2036-2045.

[30] J.L. Casaus, J.A. Navarro, M. Hervas, A. Lostao, M.A. De la Rosa, C. Gomez-Moreno, J. Sancho, M. Medina, *Anabaena* sp. PCC 7119 flavodoxin as electron carrier from photosystem I to ferredoxin-$NADP^+$ reductase. Role of Trp(57) and Tyr(94), J Biol Chem 277 (2002) 22338-22344.

[31] T. Mayoral, M. Martinez-Julvez, I. Perez-Dorado, J. Sanz-Aparicio, C. Gomez-Moreno, M. Medina, J.A. Hermoso, Structural analysis of interactions for complex formation between Ferredoxin-$NADP^+$ reductase and its protein partners, Proteins 59 (2005) 592-602.

[32] I. Nogues, M. Hervas, J.R. Peregrina, J.A. Navarro, M.A. de la Rosa, C. Gomez-Moreno, M. Medina, *Anabaena* flavodoxin as an electron carrier from photosystem I to ferredoxin-$NADP^+$ reductase. Role of flavodoxin residues in protein-protein interaction and electron transfer, Biochemistry 44 (2005) 97-104.

[33] C.G. Genzor, A. Beldarrain, C. Gomez-Moreno, J.L. Lopez-Lacomba, M. Cortijo, J. Sancho, Conformational stability of apoflavodoxin, Protein Sci 5 (1996) 1376-1388.

[34] C.G. Genzor, A. Perales-Alcon, J. Sancho, A. Romero, Closure of a tyrosine/tryptophan aromatic gate leads to a compact fold in apoflavodoxin, Nat Struct Biol 3 (1996) 329-332.

[35] D.E. Edmondson, G. Tollin, Chemical and physical characterization of the Shethna flavoprotein and apoprotein and kinetics and thermodynamics of flavin analog binding to the apoprotein, Biochemistry 10 (1971) 124-132.

[36] H.C. Gasteiger E., Gattiker A., Duvaud S., Wilkins M.R., Appel R.D., Bairoch A., Protein Identification and Analysis Tools on the ExPASy Server, Humana Press, 2005.

[37] S.G. Mayhew, Potentiometric measurement of oxidation-reduction potentials, Methods Mol Biol 131 (1999) 49-59.

[38] M. Dubourdieu, J. le Gall, V. Favaudon, Physicochemical properties of flavodoxin from *Desulfovibrio vulgaris*, Biochim Biophys Acta 376 (1975) 519-532.

[39] R.D. Draper, L.L. Ingraham, A potentiometric study of the flavin semiquinone equilibrium, Arch Biochem Biophys 125 (1968) 802-808.

[40] S.G. Mayhew, The effects of pH and semiquinone formation on the oxidation-reduction potentials of flavin mononucleotide. A reappraisal, Eur J Biochem 265 (1999) 698-702.

[41] R.F. Anderson, Energetics of the one-electron reduction steps of riboflavin, FMN and FAD to their fully reduced forms, Biochim Biophys Acta 722 (1983) 158-162.

[42] A.G.W. Leslie, Joint CCP4 + ESF-EAMCB, Newsletter on Protein Crystallography 26 (1992).

[43] N. Collaborative Computational Project, The CCP4 Suite: Programs for Protein Crystallography, Acta Cryst. D50 (1994) 760-763.

[44] A. Vagin, A. Teplyakov, MOLREP: an automated program for molecular replacement. , J. Appl. Cryst. 30 (1997) 1022-1025.

[45] A.T. Brünger, P.D. Adams, G.M. Clore, W.L. DeLano, P. Gros, R.W. Grosse-Kunstleve, J.-S. Jiang, J. Kuszewski, M. Nilges, N.S. Pannu, R.J. Read, L.M. Rice, T. Simonson, G.L. Warren, Crystallography & NMR System: A New Software Suite for Macromolecular Structure Determination. Crystallography & NMR System. , Acta Cryst. D54 (1998) 905-921.

[46] G. Murshudov, A. Vagin, E. Dodson, Refinement of macromolecular structures by the maximum-likelihood method., Acta Crystallogr D Biol Crystallogr 53 (1997) 240-255.

[47] T.A. Jones, J.Y. Zou, S.W. Cowan, M. Kjeldgaard, Improved methods for building protein models in electron density maps and the location of errors in these models Acta Crystallogr. Sect. A 47 (1991) 110-119.

[48] R.A. Laskowski, M.W. MacArthur, D.S. Moss, J.M. Thornton, PROCHECK: a program to check the stereochemical quality of protein structures. , J. Appl. Cryst. 26 (1993) 283-291.

[49] W.L. Delano, They PyMOL molecular graphics system, DeLano Scientific, San Carlos, CA, USA (2002) http://www.pymol.org.

[50] N.a.P. Guex, M.C. , SWISS-MODEL and the Swiss-PdbViewer: An environment for comparative protein modeling. , Electrophoresis 18 (1997) 2714-2723.

[51] D.A. Case, T.E. Cheatham, 3rd, T. Darden, H. Gohlke, R. Luo, K.M. Merz, Jr., A. Onufriev, C. Simmerling, B. Wang, R.J. Woods, The Amber biomolecular simulation programs, J Comput Chem 26 (2005) 1668-1688.

[52] C. Schneider, J. Suhnel, A molecular dynamics simulation of the flavin mononucleotide-RNA aptamer complex, Biopolymers 50 (1999) 287-302.

[53] V. Sobolev, A. Sorokine, J. Prilusky, E.E. Abola, M. Edelman, Automated analysis of interatomic contacts in proteins, Bioinformatics 15 (1999) 327-332.

[54] Z. Zhou, R.P. Swenson, Evaluation of the electrostatic effect of the 5'-phosphate of the flavin mononucleotide cofactor on the oxidation--reduction potentials of the flavodoxin from *Desulfovibrio vulgaris* (Hildenborough), Biochemistry 35 (1996) 12443-12454.

[55] R.D. Draper, L.L. Ingraham, The affinity of flavin semiquinones for certain aromatic compounds and disulfides, Arch Biochem Biophys 139 (1970) 265-268.

[56] J.D. Walsh, A.-F. Miller, Flavin reduction potential tuning by substitution and bending, Journal of Molecular Structure (Teochem) 623 (2003) 185-195.

[57] R.P. Swenson, G.D. Krey, Site-directed mutagenesis of tyrosine-98 in the flavodoxin from *Desulfovibrio vulgaris* (Hildenborough): regulation of oxidation-reduction properties of the bound FMN cofactor by aromatic, solvent, and electrostatic interactions, Biochemistry 33 (1994) 8505-8514.

[58] Z. Zhou, R.P. Swenson, The cumulative electrostatic effect of aromatic stacking interactions and the negative electrostatic environment of the flavin mononucleotide binding site is a major determinant of the reduction potential for the flavodoxin from *Desulfovibrio vulgaris* [Hildenborough], Biochemistry 35 (1996) 15980-15988.

[59] Z. Zhou, R.P. Swenson, Electrostatic effects of surface acidic amino acid residues on the oxidation-reduction potentials of the flavodoxin from *Desulfovibrio vulgaris* (Hildenborough), Biochemistry 34 (1995) 3183-3192.

[60] S.M. Geoghegan, S.G. Mayhew, G.N. Yalloway, G. Butler, Cloning, sequencing and expression of the gene for flavodoxin from *Megasphaera elsdenii* and the effects of removing the protein negative charge that is closest to N(1) of the bound FMN, Eur J Biochem 267 (2000) 4434-4444.

Figure Legends

Figure 1. (A) Visible difference absorption spectra of the different mutated Fld_{ox} forms relative to WT Fld_{ox}: Trp57Glu (dotted thin line), Trp57Lys (solid bold line), Trp57Arg (solid thin line), Ile59Ala/Ile92Ala (dash-dotted bold line) and Ile59Glu/Ile92Glu (dashed bold line). The spectra were recorded in 50 mM Tris/HCl, pH 8.0 at room temperature. (B) UV/Vis spectra obtained during photoreduction and redox titration of Ile59Ala/Ile92Ala Fld. Nernst plots for the (C) ox/sq and (D) sq/hq couples of different Fld forms in 50 mM Tris/HCl, pH 8.0 and 25 ºC; WT (closed square), Thr12Lys (open circle), Glu16Lys (cross), Trp57Glu (closed triangle), Trp57Lys (open triangle), Trp57Arg (open square), Ile59Ala/Ile92Ala (closed circle) and Ile59Glu/Ile92Glu (bars).

Figure 2. (A) Thermodynamic cycle showing the relationship between reduction potentials of free and bound FMN with the free energy for the interaction of ApoFld with FMN in the ox, sq and hq states. (B) Binding energy profiles versus reduction state for WT (closed square), Thr12Lys (closed triangle), Glu16Lys (open triangle), Ile59Ala/Ile92Ala (closed circle) and Ile59Glu/Ile92Glu (open circle) ApoFld:FMN complexes and (C) WT (closed square), Trp57Glu (open triangle), Trp57Lys (open circle) and Trp57Arg (closed triangle) ApoFld:FMN complexes.

Figure 3. Fld surface environment of FMN in the X-ray structures of different Fld variants: WT (1flv, [7]), Trp57Glu (2v5v), Trp57Leu (1obo, [5]) and Ile92Ala (2v5u). Electrostatic potential surface is shown for each one of the structures. FMN, Ile59, Asn58, Trp57 (or the corresponding mutant) and Ile92 (or the corresponding mutant) positions are shown as sticks. In the case of the mutants positions of WT Fld FMN, Trp57, Asn58, Ile59 and Ile92 are also shown for comparison. Sticks are colored in

CPK with the carbon atoms in green for WT and either blue or yellow for the mutants. The position of the water molecule interacting with the PO2 of FMN is shown for the structures of Trp57Glu and Trp57Leu. The H-bonds involving this water molecule are shown as a dashed line.

Figure 4. Relative disposition between the flavin ring and the 50's loop in the X-ray structures of the different Fld variants. Superposition onto WT Fld (CPK, green C atoms) for (A) the Trp57Glu (CPK, C in orange) and (B) the Ile92Ala (CPK, C in orange) Fld structures. Relative orientations and distances for the NH group of the residue 59 with regard to N5 of the isoalloxazine are shown in detail. The water molecule H-bonding PO2 and the Glu57 is also shown.

Figure 5. Plot of the solvent accessibility of the isoalloxazine ring (●) and the 8-CH_3 group (○) of FMN *versus* (A) $E_{ox/sq}$ and (B) $E_{sq/hq}$ for mutants of *Anabaena* Fld. In (B) the solid and dotted lines indicate correlation fitting of the isoalloxazine and methyl group, respectively. Solvent accessibility data refer to crystal structures for those Fld variants with available data (it is remarkable that very similar values were obtained for the corresponding models). For the rest of the Fld variant solvent accessible data refer to the model constructed as reported in the materials and methods section.

Table

Table 1. Structure determination and statistics for Trp57Glu and Ile92Ala Fld mutants.

	W57E	I92A
Data collection statistics		
Space group	$P2_1$	C2
Unit cell parameters		
a, Å	37.85	110.96
b, Å	55.58	37.49
c, Å	70.26	90.60
β, °	91.17	123.66
Wavelength, Å	1.5418	1.5418
Resolution, Å	25.48-1.88 (1.98-1.88)	25.69-1.99 (2.10-1.99)
Total no. of reflections	185239	71262
No. of unique reflections	23136	21357
Redundancy	3.6 (3.3)	9.9 (4.6)
Completeness, %	96.8 (96.8)	94.4 (83.2)
I/σ	9.5 (3.6)	20.0 (4.3)
R_{merge} [a]	0.053 (0.192)	0.078 (0.367)
Refinement statistics		
Resolution range, Å	25.48-1.88	25.69-1.99
Protein non-hydrogen atoms	2643	2642
Metal atoms	1	-
Ligand non-hydrogen atoms	62	62
Solvent non-hydrogen atoms	240	198
R_{work}	0.18	0.19
R_{free} [b]	0.22	0.27
rmsd bond lenght, Å	0.019	0.025
rmsd bond angles, °	1.6	2.1
Average B-factor, $Å^2$	29.73	24.48

Values in parentheses correspond to the highest resolution shell.

[a] $R_{sym} = \Sigma|I-I_{av}|/\Sigma I$, where the summation is over symmetry equivalent reflection
[b] R calculated for 7% of data excluded from the refinement.

Table

Table 2. UV-Visible spectral properties of WT and mutated Flds in the oxidized and semiquinone states. Data obtained in 50 mM Tris/HCl, pH 8.0 at 25 ºC.

Fld form	oxidized					Isosbestic points ox-sq (nm)	semiquinone	
	λ_{max} (nm)		ε_{max} ($mM^{-1}cm^{-1}$)				λ_{max} (nm)	ε_{max} ($mM^{-1}cm^{-1}$)
	I	II	I	II	$\varepsilon_I/\varepsilon_{II}$			
WT[a]	463	374	8.8	8.1	1.08	516	578	5.0
T12K	464	373	9.0	8.25	1.09	516	578	4.9
E16K	464	373	8.7	8.15	1.07	516	580	4.8
W57E	456	371	9.3	8.7	1.07	506	572	4.9
W57K	459	372	9.1	8.9	1.02	509	576	4.9
W57R	456	369	9.1	8.5	1.07	506	575	4.6
I59A/I92A	463	373	8.7	7.6	1.15	517	580	4.5
I59E/I92E	464	374	8.3	7.4	1.12	516	579	4.3

[a] Data from [24] and [6].

Table

Table 3. Midpoint reduction potentials for the different Fld forms. Data obtained in 50 mM Tris/HCl, pH 8.0, at 25 ºC.

Fld form	$E_{ox/sq}$ (mV)	$E_{sq/hq}$ (mV)	$\Delta E_{ox/sq} - \Delta E_{ox/sq,WT}$ (mV)	$\Delta E_{sq/hq} - \Delta E_{sq/hq,\ WT}$ (mV)
WT[a]	-266	-439	-	-
T12K	-252	-438	14	1
E16K	-254	-440	12	-1
W57E	-255	-419	11	20
W57K	-188	-410	78	29
W57R	-228	-390	38	49
W57A[b]	-232	-417	34	22
W57F[b]	-211	-437	55	2
W57L[b]	-271	-407	-5	32
W57Y[b]	-198	-447	68	8
I59A/I92A	-337	-391	-71	48
I59E/I92E	-318	-422	-52	17
FMN free[c]	-365	-117	-99	322

[a] Data from [24].

[b] Data from [9]. Data for these Fld forms were originally determined at pH 7.0. These values were corrected applying a change of -59 mV/pH unit to estimate $E_{ox/sq}$ ($E_{sq/hq}$ was assumed to be pH independent above pH 7.0).

[c] $E_{ox/sq}^{free}$ and $E_{sq/hq}^{free}$ calculated from equations 5 and 4 from [40], respectively (pH 8.0 and 22ºC), as explained in Materials and Methods.

Table

Table 4. Dissociation constants for the ApoFld:FMN_{ox} complexes and free energies for the formation of the corresponding oxidized, semiquinone and hydroquinone complexes. Data obtained in 50 mM Tris/HCl, pH 8.0 at 25 ºC.

Fld form	K_d (nM)[a]	ΔG_{ox} (Kcal mol^{-1})[b]	ΔG_{sq} (Kcal mol^{-1})[c]	ΔG_{hq} (Kcal mol^{-1})[c]
WT	1.2	-12.16	-14.45	-7.02
T12K	9.0	-10.97	-13.58	-6.17
E16K	1.1	-12.21	-14.77	-7.33
W57E	4.8	-11.34	-13.88	-6.91
W57K	10.1	-10.90	-14.98	-8.23
W57R	9.5	-10.94	-14.10	-7.80
I59A/I92A	3.5	-11.53	-12.17	-5.86
I59E/I92E	3.8	-11.48	-12.56	-5.53

[a] Determined from fluorometric titrations of FMN_{ox} with WT or mutated ApoFlds.

[b] Calculated from data in[a] using the equation $\Delta G_{ox} = -RT \ln 1/K_d$

[c] Calculated as described from equations 3 and 4 [9], with $E_{ox/sq}^{free}$ and $E_{sq/hq}^{free}$ from table 3.

Figure 1

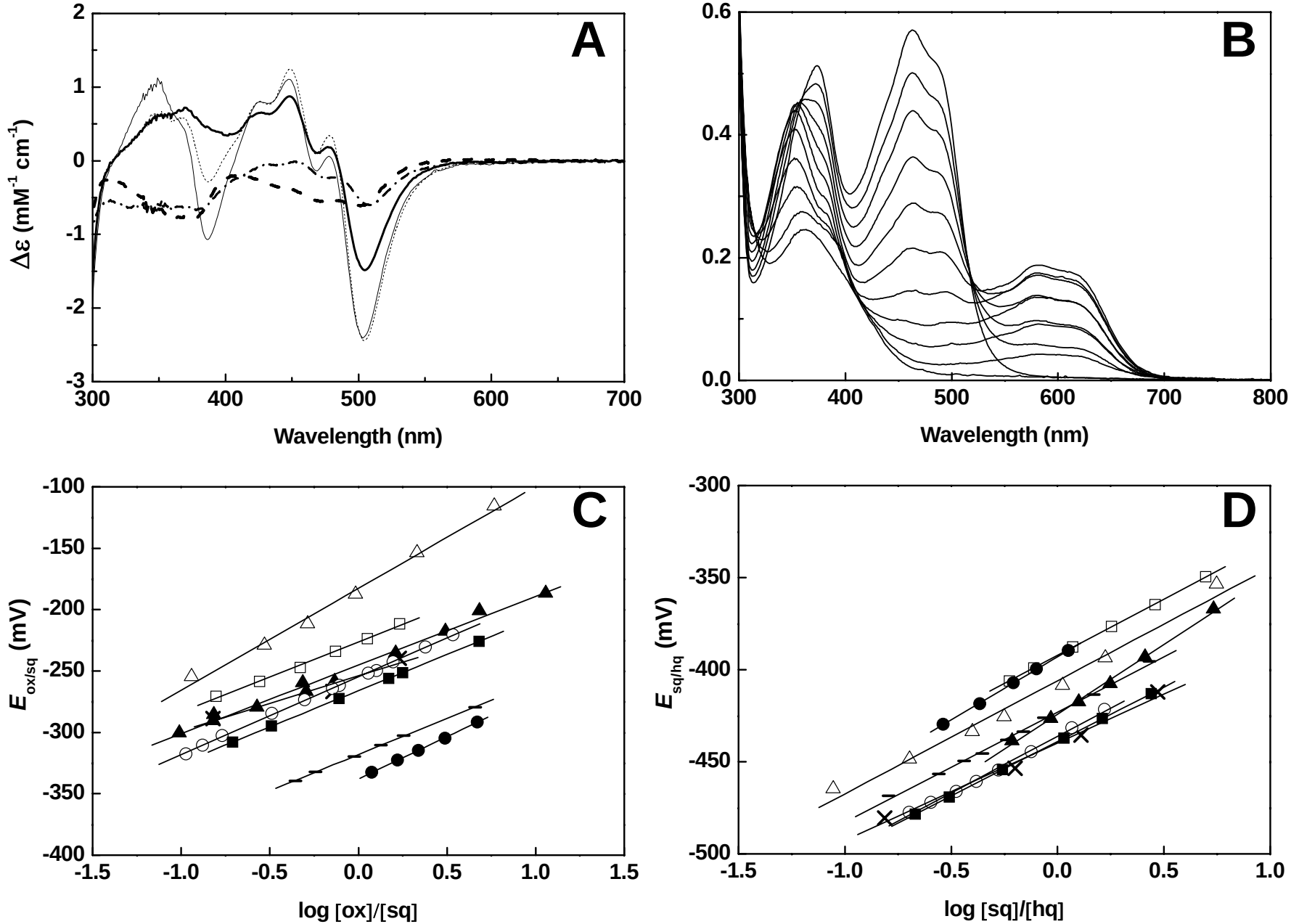
A
Δε (mM-1 cm-1)
Wavelength (nm)
B
Wavelength (nm)
C
Eox/sq (mV)
log [ox]/[sq]
D
Esq/hq (mV)
log [sq]/[hq]

Figure 2

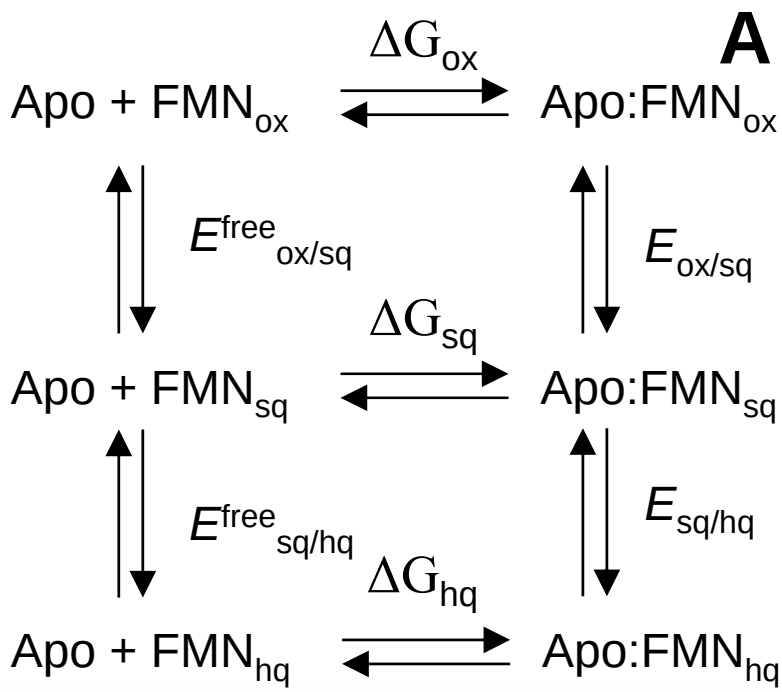
A
ΔG_ox
Apo + FMN_ox
Apo:FMN_ox
E^free_ox/sq
E_ox/sq
ΔG_sq
Apo + FMN_sq
Apo:FMN_sq
E^free_sq/hq
E_sq/hq
ΔG_hq
Apo + FMN_hq
Apo:FMN_hq

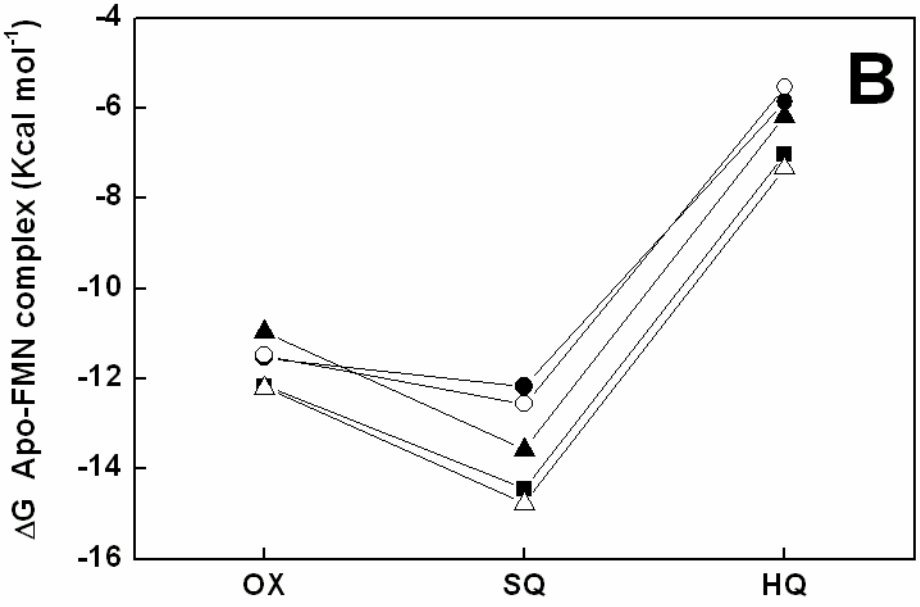
B
ΔG Apo-FMN complex (Kcal mol-1)
-4
-6
-8
-10
-12
-14
-16
OX
SQ
HQ

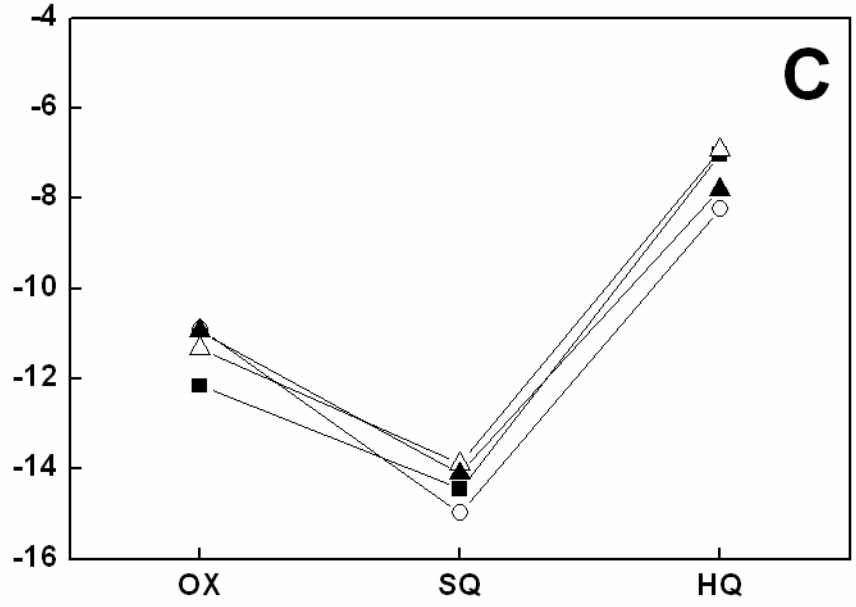
C
-4
-6
-8
-10
-12
-14
-16
OX
SQ
HQ

Figure 3

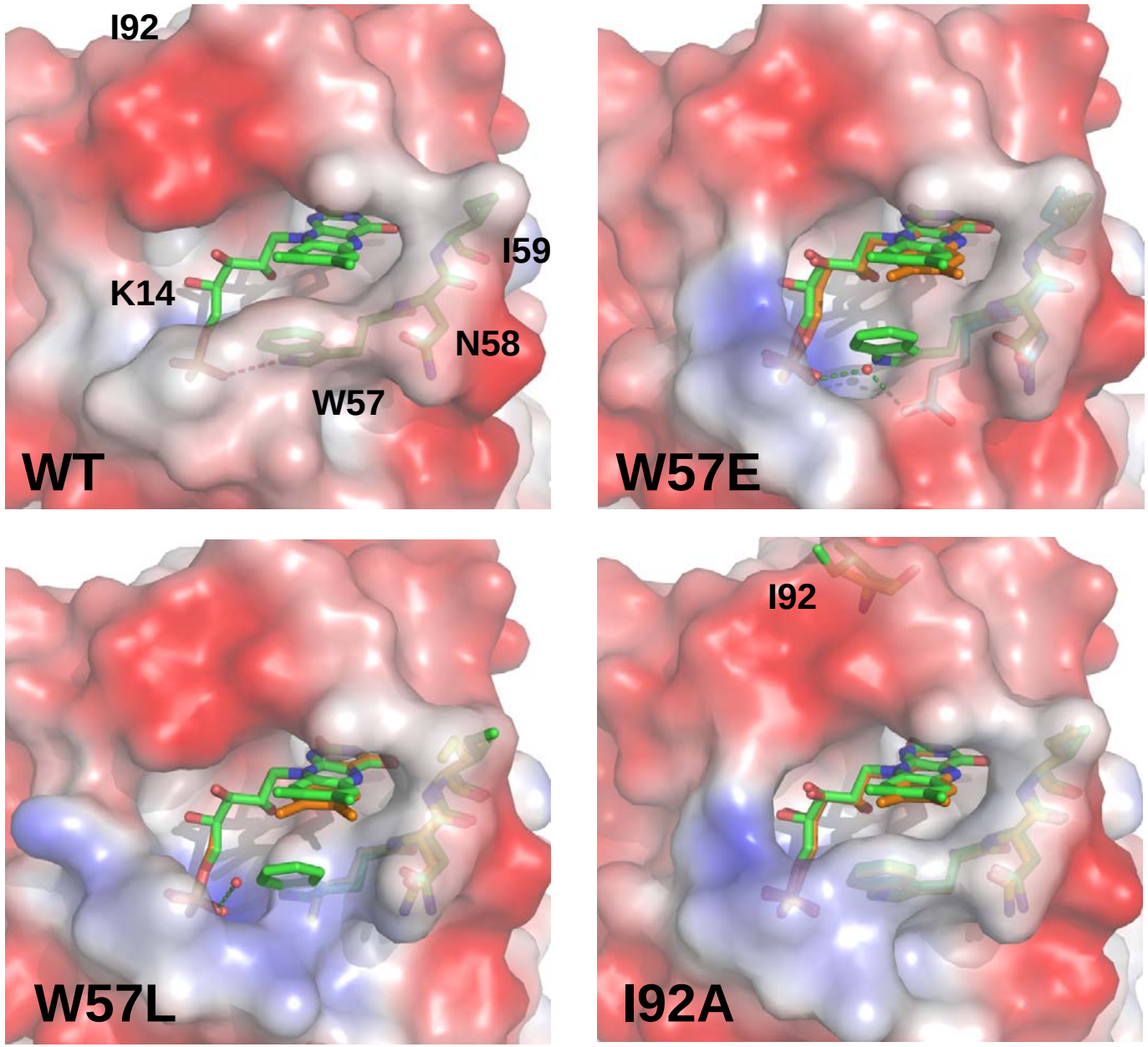

Figure 4

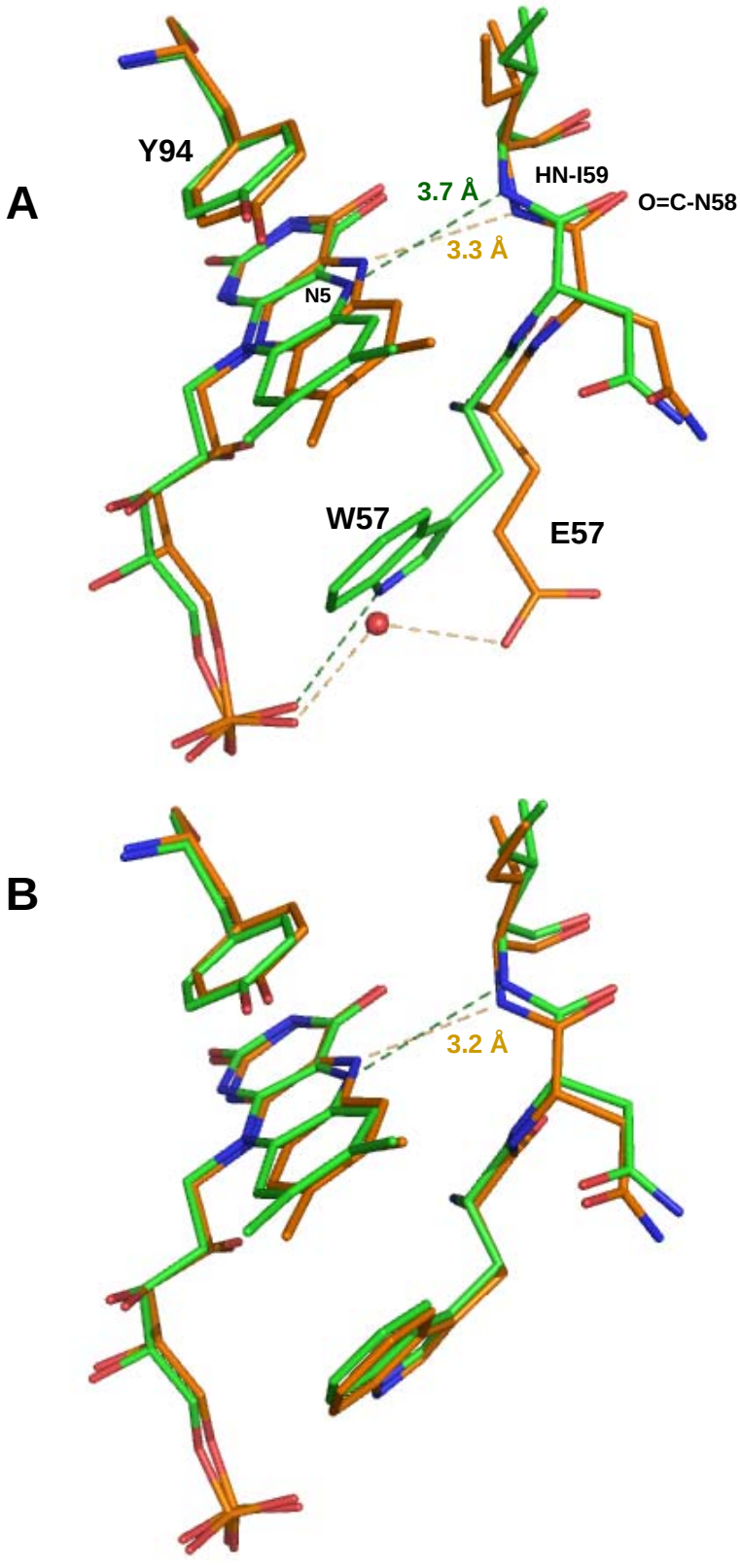

Figure 5

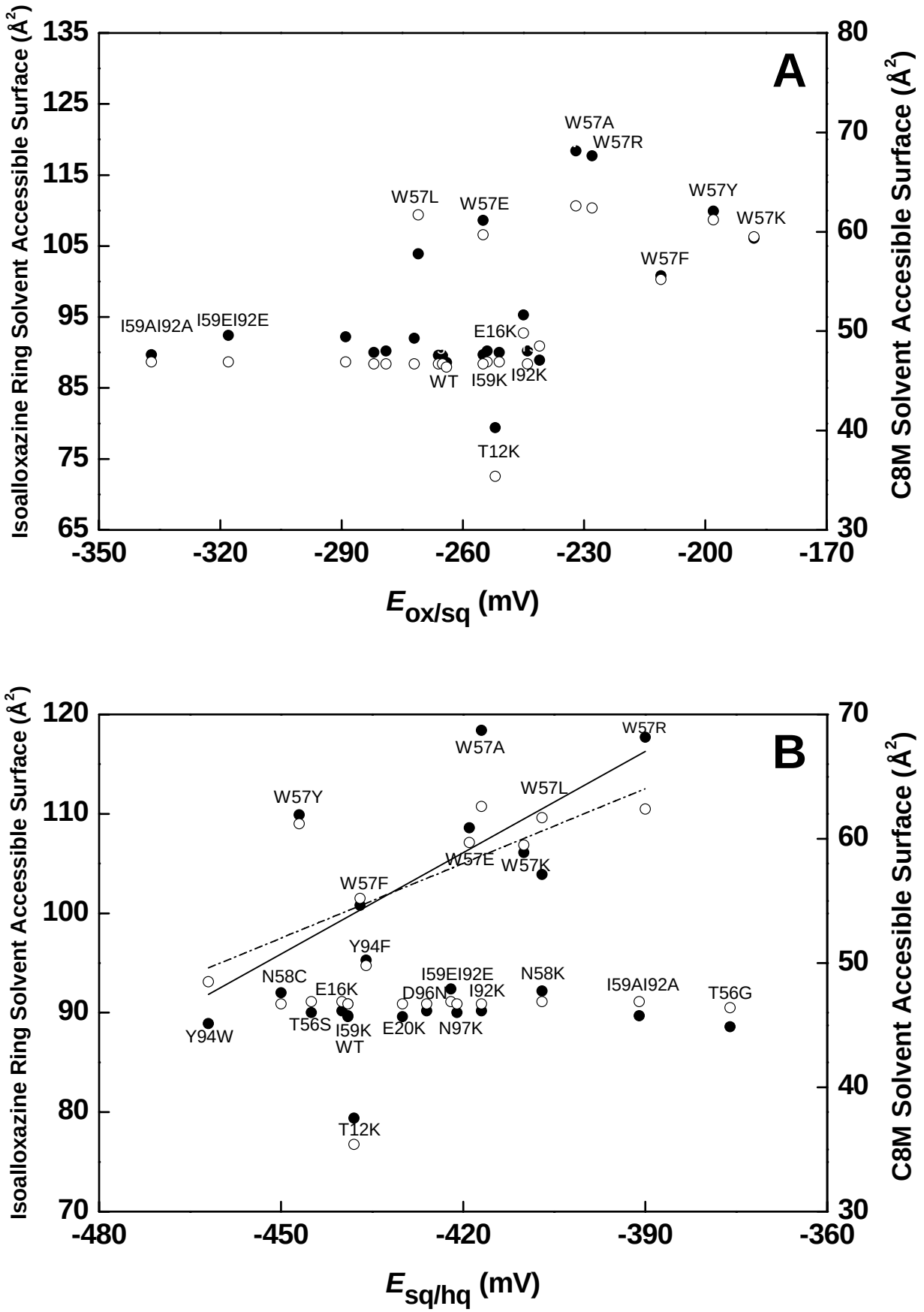
A
Isoalloxazine Ring Solvent Accessible Surface (Å²)
C8M Solvent Accesible Surface (Å²)
E_ox/sq (mV)
W57A
W57R
W57L
W57E
W57Y
W57K
W57F
I59AI92A
I59EI92E
E16K
WT
I59K
I92K
T12K
B
Isoalloxazine Ring Solvent Accessible Surface (Å²)
C8M Solvent Accesible Surface (Å²)
E_sq/hq (mV)
W57A
W57R
W57Y
W57L
W57E
W57K
W57F
Y94F
N58C
E16K
I59EI92E
D96N
I92K
N58K
I59AI92A
T56G
Y94W
T56S
I59K
WT
E20K
N97K
T12K